Experimental and high-order LES analysis of the flow in near-wall region of a square cylinder

M. Minguez [a], C. Brun [b], R. Pasquetti [c], E. Serre [d,*]

[a] *Seal Engineering, Centre Atria, 5 Bd de Prague, Nîmes, France*
[b] *LEGI, UMR CNRS 5519, Université Joseph Fourier, Grenoble, France*
[c] *Lab. J.-A. Dieudonné, UMR CNRS 6621, Université de Nice-Sophia Antipolis, France*
[d] *M2P2, UMR CNRS 6181, Aix-Marseille Université, France*

A coupled experimental/numerical analysis of turbulent flow past a square cylinder is performed at the ERCOFTAC Reynolds number $Re = U_\infty D/\nu = 21{,}400$, where U_∞ is the inflow velocity and D the cylinder height. Complementary Laser Doppler Velocimetry (LDV) and high-order large-eddy simulations (LES) approaches, based on a spectral vanishing technique (SVV-LES), provide a comprehensive data base including both instantaneous data and post-processed statistics. Beyond these results, an achievement of the paper is to investigate the coherent structures developing on the sides and in the wake of the cylinder with a special focus on the flow features in the near-wall region. The flow is found to separate at the leading edge of the cylinder with the occurence of three-dimensional Kelvin–Helmholtz (KH) pairings localized in the separating shear layer. The interaction between these KH vortical structures and Von Kármán vortex shedding (VK) in the near wake is discussed based on both visualisations and frequency analysis. In particular, signatures of VK and KH vortical structures are found on velocity time samples.

1. Introduction

Flows over bluff bodies are related to many practical applications and are currently subject to industrial investigations. In this framework, the turbulent flow behind a cylinder is thus of great interest since it constitutes a generic configuration with many applications in fields such as external aerodynamics, offshore engineering or environmental sciences.

As it is typical for bluff body wakes, drag prediction and its control are among the main objectives of aerodynamics studies. However, the flow that develops over this geometry is very complex because it is fully three-dimensional, unsteady, including transition regions to turbulence as well as flow separations along the sidewall. Since the pressure field changes rapidly near the separation and reattachment points, its prediction is decisive for a correct estimation of the drag and lift coefficients.

The formation of a vortex street is generally considered to be the result of a coupling between Kelvin–Helmholtz (KH) instabilities within the separated shear layers and the Von Kármán (VK) instability in the near wake. In each shear layer above and below the cylinder, the instabilities lead to vortex-sheet roll-up that favors the multi-scales feature of the flow.

There has been some studies on the flow past a rectangular cylinder even if most of works have been done on the flow past a circular cylinder (see a review in Williamson (1996)). Lyn and Rodi (1994) performed experiments for the flow past a square cylinder at relatively high Reynolds number, $Re = 21{,}400$. In their study, they focused on the shear layer formed by flow separation from the upstream corner of a square cylinder rather than on the near-wake region. Okajima (1982) carried out experiments on the flow past a rectangular cylinder of diverse aspect ratio (1, 2, 3, and 4) at various Reynolds in the range (70–20,000), and determined how Strouhal number St varies with Reynolds number Re.

The interaction of coherent structures has been studied both experimentally and numerically but mainly in the frame of the wake behind a circular cylinder. A special focus was given to the controversial conclusions of the pioneer works of Bloor (1964): The ratio from the shear layer frequency to the fundamental VK frequency is quasi-proportional to $\sqrt{Re}$. Direct comparisons between numerical (DNS) and experimental (PIV) studies have been performed by Dong et al. (2006) for the circular cylinder wake. In the particular case of a square cylinder wake, experimental and numerical works exist, Brun and Goossens (2008), Brun et al. (2008), Patankar and Kelkar (1992). They have focused on the interaction of these coherent structures in the near wake to recover the Reynolds dependent instabilities scenario initially detailed by Bloor (1964), Wei and Smith (1986) and recently Rajagopalan and Antonia (2005) for the circular cylinder.

* Corresponding author.
E-mail address: serre1@l3m.univ-mrs.fr (E. Serre).

Separation of the flow, large scale eddying turbulent structures that dominate the turbulent transport, unsteady processes such as vortex shedding, and transition from laminar to turbulent flow which can happen in various ways make this flow very challenging for numerical modeling. This motivated two ERCOFTAC benchmarks (Rodi, 1993; Voke, 1996) at the Reynolds number $Re = 21{,}400$ providing a large data base for the validation of turbulence modeling.

Various studies have demonstrated the inability of classical RANS modeling using various eddy-viscosity models to render the fundamental physics of such flows with in general an underprediction of the turbulence fluctuations. Bosch and Rodi (1996, 1998) have observed that the standard k–ϵ model underpredicts severely the strength of the shedding motion and the vortex shedding frequency is lowered, mainly because of the excessive turbulent kinetic energy production in the stagnation region. The Kato modification of the k–ϵ model avoids this problem especially when it is combined with the two-layer approach resolving the near-wall region as shown for a square cylinder close to a wall in Bosch and Rodi (1996). Advanced recent RANS practices, i.e. explicit algebraic stress model, can superficially provide many features of the flow (Lübcke et al., 2001) but even if they considerably improved the results of classical RANS models they slightly underpredict the intensity of the transient motion and finally do not provide the same level of agreement with experimental measurements as achieved by the LES. Reynolds-stress models yield significantly improved predictions for the square cylinder shedding flow but even if they provide a correct distribution of laminar and turbulent regions they tend to overpredict the periodic motion (Franke and Rodi, 1991). As pointed out by Iaccarino et al. (2003), using the $v2-f$ turbulence model, unsteady RANS modeling brings a global improvement in the results by integrating the periodic vortex shedding motion in the averaged flow field. In contrast to this, the computationally more demanding large-eddy simulation (LES) is known to be a viable approach to simulate unsteady flows. Nevertheless, none of the LES results are uniformly good and there can be large differences between the results, mainly because LES is strongly dependent of the numerical modeling like the resolution (especially in the spanwise direction) or the numerical dissipation of the scheme (see a review in Rodi (1993)). During the ERCOFTAC benchmark (Voke, 1996), comparisons of several SGS models provided the conclusion that the Lagrangian Dynamic mixed model was the most suited since it provided the best overall agreement with the experiment of reference and good calculation stability due to the efficient stabilization by averaging over particle trajectories. Later, Sohankar et al. (2000) using a dynamic model with one equation seemed to provide one of the best agreement with experimental measurements of Lyn et al. (1995) in the frame of the ERCOFTAC benchmark highlighting the three-dimensional effects in this flow.

In the present paper, a complementary Laser Doppler Velocimetry (LDV) and a high-order LES approach has been performed at Reynolds number $Re = 21{,}400$. In the framework of high-order approaches, the Spectral Vanishing Viscosity (SVV) methodology offers a promising way to perform LES of flows over bluff bodies (Minguez et al., 2008). The SVV allows to dissipate the energy accumulated on the highest spatial wave numbers of the flow preserving the spectral accuracy as soon as the solution is smooth. Experimental set up and numerical modeling are first presented. Comparative results are presented showing a satisfactory agreement in the turbulence quantities. Both the high resolution of the LDV experiments and the low-dissipation properties of SVV-LES allows to investigate the flow features in the near-wall region of a square cylinder. Turbulent structures visualizations of KH anf VK instabilities as well as long data recording performed with LDV and SVV-LES are finally provided.

2. Experimental facility

Experiments were conducted at Orléans Prisme institute, in a low speed looped-wind tunnel (Fig. 1) with a $L_y \times L_z = 2\text{ m} \times 2\text{ m}$ test section (Fig. 2). A square cylinder with a diameter $D = 100$ mm was placed at a distance $x - x_o = 20D$ downstream of the contraction outlet. The size of the test section yields a sufficient aspect ratio $L_z/D = 50$ to obtain a wake development with negligible end effects. It could be compared to an aspect ratio of 9.75 for Lyn et al. (1995) or 6 for Durao et al. (1988). The blockage effect was only $D/L_y = 5\%$ in the present experiments compared to 7 % for Lyn et al. (1995) or 14 % for Durao et al. (1988). Thanks to the use of a settling chamber and a sufficient section contraction of about 6.25:1 (real contraction ratio of 6.25) above the test section, the measured velocity profiles at midspan had less than $\langle U\rangle/U_\infty = 0.5\%$ of spatial non-uniformity and less than $u'/U_\infty = 0.8\%$ of turbulence level. It was about 2% for Lyn and Rodi (1994) experiments. Two sets of experiments were performed to provide both statistics profiles and energy density spectra at a mean flow velocity ranging from $U_\infty = 3.07$ m/s to $U_\infty = 3.3$ m/s, which yields a Reynolds number of about $Re = 20{,}000$–$22{,}000$.

Non-intrusive velocity measurements were performed using a two components Laser Doppler Velocimetry LDV system which consisted of a Dantec bichromatic Argon laser with a size of the measuring volume at the intersection of two laser beams $Lo \times ho \times ho = 1.74\text{ mm} \times 90.5\mu\text{m} \times 90.5\mu\text{m}$, and a beam fringe spacing $i = 3.74$ μm. The beams half angle is about 4 degrees and the lens focal distance is 1.20 m. Two Dantec BSA processors are used.

Non-intrusive properties of the LDV technique allowed to investigate the full recirculation zone on the sides of the cylinder. The boundary layer thickness is about 1cm at the cylinder impingement. Measurements were performed down to $y = 1$ mm close to the cylinder wall, that is to say $y/D = 1\%$. The near-wall region is thus very well described and the recirculation region around the cylinder could be much better analyzed than in Lyn et al. (1995) experiments in a water tank.

The flow was seeded with DEHS particles ($C_{26}H_{50}O_4$) of very small size about 0.2–0.3 μm compared to the beam frange spacing (1/10) and low density with a high refraction coefficient (about 1.45) which compensates their very small size. Multi measurements per burst were automatically rejected by setting the maximum threshold of backscatter light from the measurement volume. This was useful to obtain high frequency samples of about 10–20 KHz and provide a sufficient frequency window of analysis to precisely describe both VK and KH vortical structures. It has never been obtained in such experiments till now. Long time samples of about 300 s each have been stored to reach more then 1000 periods of vortex shedding. Due to a saturation of the energy spectra at high frequency range a postprocessing procedure has been performed to remove the non-physical contribution to the energy spectra when computing rms values. Such a procedure consists of replacing the high frequency part of the energy signal by a spectrum with a $f^{-5/3}$-law, that is to say troncating the overcontribution

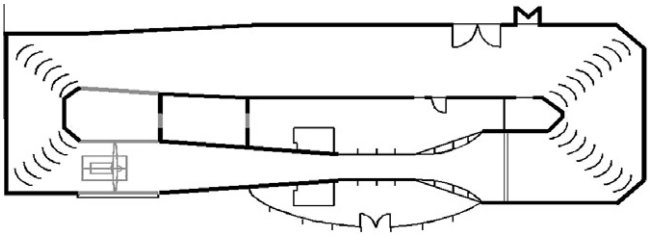

Fig. 1. Prisme Institute low speed wind tunnel in Orléans, France.

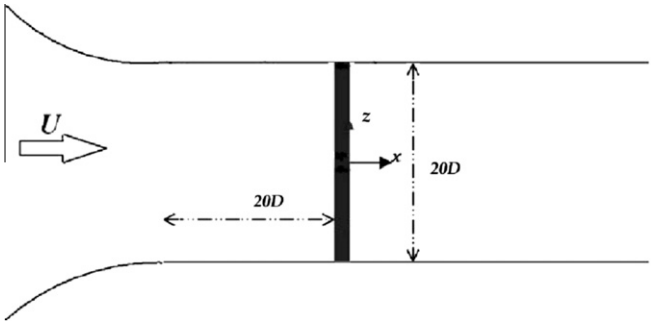

Fig. 2. LDV measurements. Tests section geometry. $H = 20D$; $l = 20D$.

of the signal to the energy spectrum. This was the case for regions where transition to turbulence occurs leading to strong non linear interactions and large increase of the fluctuation level of the signal.

3. Numerical modeling

The geometry corresponds to the one proposed by the ERFOCTAC test case (Voke, 1996). A square cylinder of height D is placed at the origin of the coordinate system within a computational domain of extension $(-4.5D, 15D) \times (-7D, 7D) \times (-2D, 2D)$ respectively in the (x, y, z) directions. That corresponds to a transverse blockage effect of $D/L_y = 7.1\%$ slightly larger than in the present experiments, performed with a blocking factor (ratio between the bluff body section to the channel one) of 1.8%.

The flow is governed by the incompressible Navier-Stokes equations written in the velocity–pressure formulation. At the inlet, an uniform velocity profile U_∞ is imposed, whereas the outlet is treated by convective condition. The spanwise direction is assumed to be homogenous. A penalization technique (Minguez et al., 2008) is used to model the square cylinder so that the no-slip boundary condition at its surface is implicitly expressed. D, U_∞ and D/U_∞ define the characteristics length, speed and time, respectively.

The numerical modeling is the SVV-LES methodology described in Pasquetti et al. (2008) and already successfully applied on the ERCOFTAC test of the Ahmed body (Minguez et al., 2008). The scheme is globally second-order accurate in time and the space approximation in space is spectral with a Fourier–Galerkin method in the homogeneous spanwise direction (z-direction) and a Chebychev-collocation method in the non-homogeneous streamwise and crossflow directions (x and y-directions).

The present LES methodology is performed through a Spectral Vanishing Viscosity (SVV) technique (see Pasquetti et al. (2008) and Minguez et al. (2008) for details) that allows to stabilize the computation together with preserving the exponential rate of convergence of spectral methods. A SVV stabilized diffusion operator Δ_{SVV} is implemented by combining the diffusion and stabilization SVV terms to obtain:

$$\nu\Delta_{SVV} \equiv \nu\Delta + \nabla \cdot (\varepsilon_N Q_N \nabla) = \nu\nabla \cdot S_N \nabla \tag{1}$$

where ν is the kinematic viscosity and where:

$$S_N = diag\left\{S^i_{N_i}\right\}, \quad S^i_{N_i} = 1 + \frac{\varepsilon^i_{N_i}}{\nu} Q^i_{N_i} \tag{2}$$

with $\varepsilon^i_{N_i}$ an amplitude coefficient and $Q^i_{N_i}$ a 1D viscosity operator acting in direction i. Omitting for simplicity the index i, the spectral operator Q_N is defined in spectral space by a set of multiplicative coefficients, say $\widehat{Q}_k$, of the (Fourier or Chebyshev) spectrum. To this end we use the smooth function: $\widehat{Q}_k = 0$, if $0 \leqslant k < m_N$ and $\widehat{Q}_k = \exp(-(k-N)^2/(k-m_N)^2)$ if $m_N \leqslant k \leqslant N$, where m_N is the threshold frequency above which the SVV stabilization acts.

Outside the boundary layer, the SVV stabilized Laplacian Δ_{SVV} is defined with parameters $m_N = \sqrt{N}$ and $\varepsilon_N = 1/N$, independently of the spatial (x, y, z) direction. Around the square cylinder, the boundary layers being too thin to be resolved, a near-wall treatment has been developed as proposed in Minguez et al. (2008). The SVV dissipation is locally relaxed within the boundary layer through the activation parameter m_N. To this end, the SVV stabilized Navier-Stokes equations are completed with an additional boundary layer (BL) force term defined as $f_{BL} = \nu\chi_{BL}(\Delta^{BL}_{SVV} - \Delta_{SVV})\mathbf{u}$ where $\mathbf{u}$ is the velocity and with χ_{BL}, a new characteristic function equal to 1 in the near-wall region and to 0 elsewhere. Improvements of the results have been obtained by using a Δ^{BL}_{SVV} operator, with an anisotropic set of $m_N = \{2\sqrt{N_x}, 5\sqrt{N_y}, 4\sqrt{N_z}\}$ and again $\varepsilon_N = 1/N$.

The entire domain is decomposed in the x-streamwise direction in eight sub-domains with the interfaces located at $x/D = (-4.5,\ -2,\ -0.55,\ 0.55,\ 2,\ 4.5,\ 7.5,\ 10.5,\ 15)$ (Fig. 3). The usual grid (grid-1) in each subdomain is of $N = \{40, 500, 32\}$, in the x-streamwise, y-vertical and z-spanwise directions, respectively. Using a mapping in the y-vertical direction, the first grid point is located at a distance of $\Delta y/D = 0.01$ that corresponds in wall unit to $y^+ \approx 6.5$ whereas in the spanwise direction the resolution is of $\Delta z/D = 0.125$ that offers a relatively accurate description of the boundary layer, as already mentioned in the conclusions of the ERCOFTAC test case (Voke, 1996). The associated dimensionless time-step is equal to $\Delta t = 3 \times 10^{-3}$. After the time-dependent flow had settled at a statistically steady state, turbulence statistics have been averaged both in the spanwise direction and in time during 13 vortex shedding as preconized in Voke (1996). The statistical steady state is expected to be reached when the fluctuations of the averaged values in time are less than 1%. That required about 300 CPU hours on vector computer, the CPU time for one time-step being around 9 s, *i.e.* approximately 10^{-7} s per iteration and degree of freedom. Starting from an interpolation of the converged computations on (grid-1), computations have been performed over five additional vortex shedding on a finer grid in the spanwise direction (grid-2) such that N={40, 800, 128}. An averaging process using this grid would have been too expensive but such a computation provides a more detailed picture of the instantaneous flow structures.

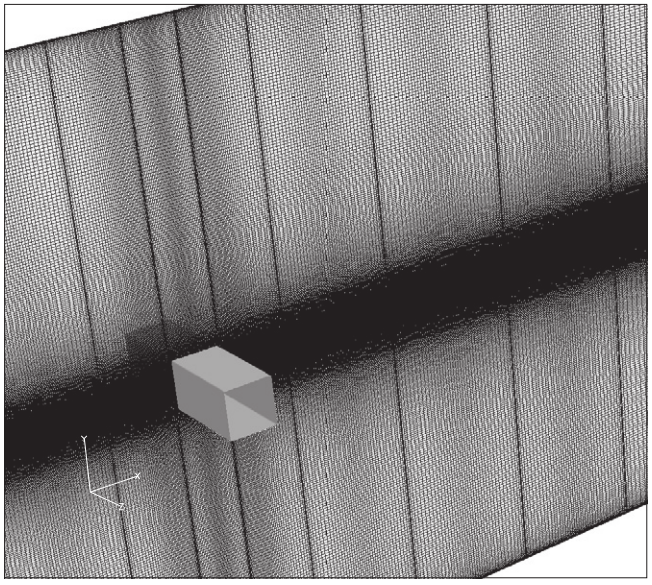

Fig. 3. Multi-domain decomposition showing the grid points distribution in the xy-plane.

4. Mean flow and turbulence statistics

Present experimental and numerical results are validated with respect to the two results of reference (Lyn et al., 1995; Rodi, 1993). The mean streamwise component of the velocity, the streamwise normal and the shear Reynolds stresses are plotted in Fig. 4 at two locations $x/D = -0.125$ and $x/D = 0.125$ corresponding to the upstream and the downstream part of the cylinder upper surface, respectively.

All the results show a satisfactory agreement except on the shear Reynolds stress which is about one order of magnitude below the normal stress. The larger number of points in the very near-wall region illustrates the finer resolution used in LDV measurements with respect to the experiment of Lyn et al. (1995). Present measurements extend earlier work especially with resolving the shear stress in the very near-wall region. All the approaches predict the same wall boundary layer thickness at both locations. SVV-LES calculations and measurements of Lyn et al. (1995) predict a slightly smaller velocity maxima than the LDV and the LES of Rodi (1993). All the approaches predict the maximum Reynolds stresses within the shear layer with a tendency for SVV-LES to overpredict the turbulence intensity at these two locations. It is debatable whether either of the two LES results provides the best agreement when all graphs are considered critically. Overall, the LES of Rodi (1993) provides a better prediction of the shear layer but the very near-wall region seems better described by SVV-LES.

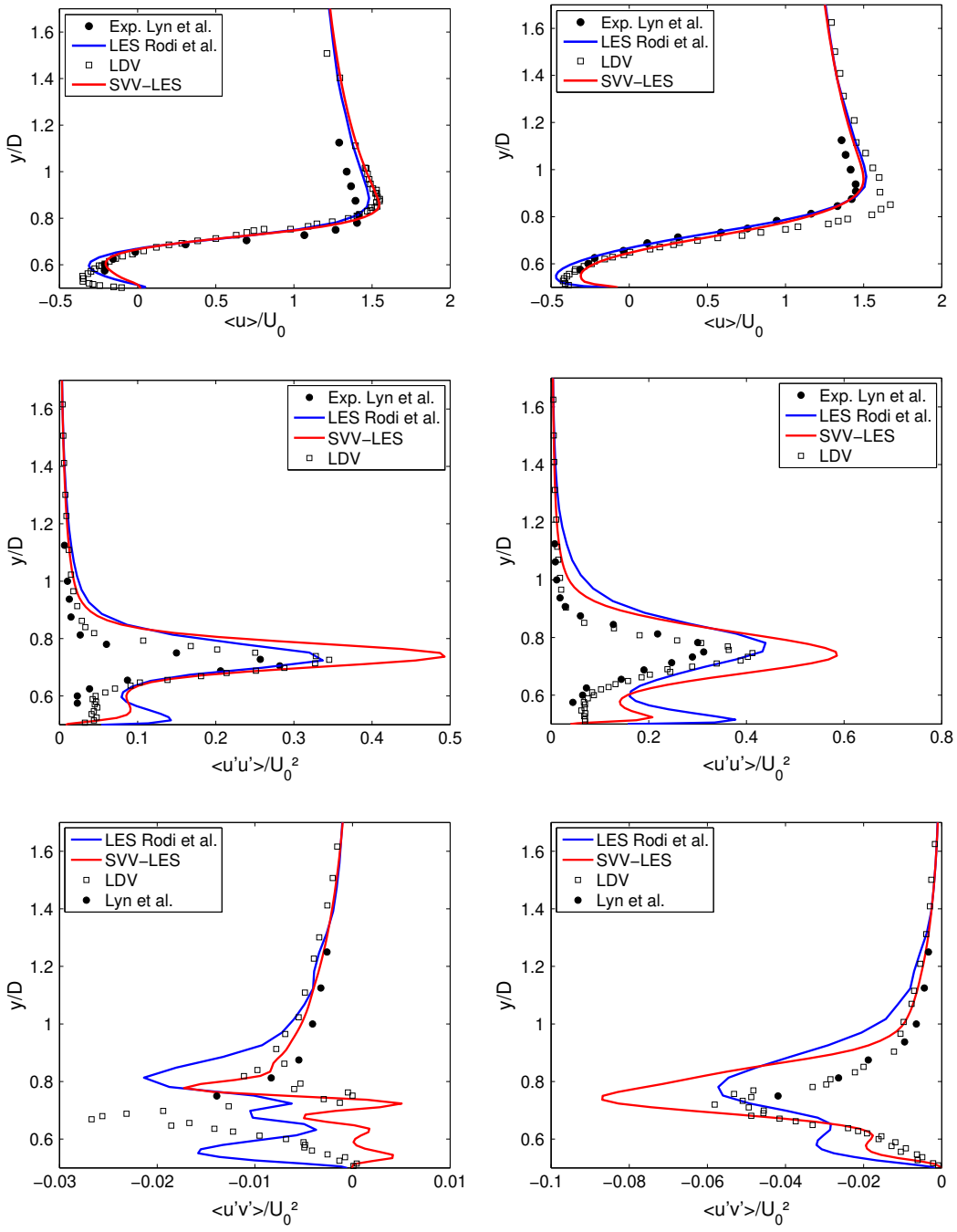

Fig. 4. Profiles of the streamwise mean velocity component (top), normal (middle) and shear Reynolds stresses (bottom) at two locations $x/D = -0.125$ and $x/D = 0.125$. Comparisons of the present LDV and SVV-LES (grid-1) results with those of references Lyn et al., 1995, 1993.

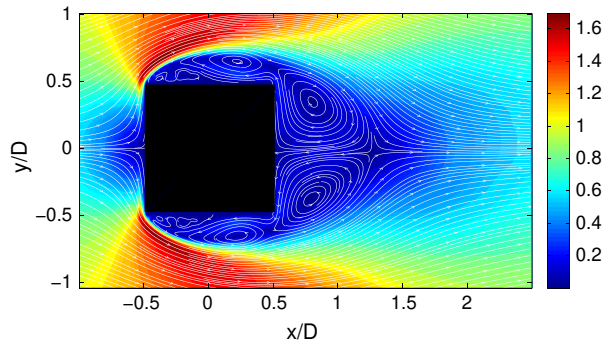

Fig. 5. Mean streamlines and isosurfaces of mean streamwise velocity U/U_∞ around the cylinder in the xy-plane at $z = 2D$ by SVV-LES (grid-1).

The topology of the mean flow is shown by streamlines of the averaged flow field in Fig. 5. In the front of the body, there is a viscosity dominated flow that impinges the cylinder at a time-averaged position $y = 0$. At the upstream corners, the flow totally separates involving near the upper and lower faces of the cylinder recirculating regions spreading on the cylinder length. Differently to the circular cylinder, the adverse pressure gradient is induced by the high streamline curvature at the sharp corners of the square cylinder that fix the points of separation. A pair of counter-rotating vortices is also identified downstream of the obstacle that combines with the recirculation over the upper and lower faces of the cylinder. As expected by the Gerrard mechanism's (Gerrard, 1966), these downstream vortices are the result of vortices developing within the shear layer that grow enough by gaining circulation from it, to draw the opposing shear layer across the near wake. Within the downstream of the large separation bubble, averaged streamlines show smaller vortical structures traveling upstream within the thin boundary layer over the cylinder.

A more quantitative description of the mean flow topology is given by the distribution of the mean velocity profiles over the surface cylinder (in Fig. 6). They were determined every 0.1D at several locations along the streamwise side face of the cylinder down to the first point at about $y/D = 0.51$. Profiles are plotted in log-scale to focus on the recirculation at the very near-wall region. The position of the mean shear layer is clearly identified. The maximum streamwise velocity is about $1.5U_\infty$ in the external part of the shear layer and slightly increases over the cylinder sidewall. Within the recirculations, the maximum evolves from $-0.15U_\infty$ to $-0.4U_\infty$.

Contrary to LES predictions, the measured mean streamwise velocity does not change sign over the cylinder surface indicating that the two bubbles traveling upstream in Fig. 5 are not observed in present experiments. Slightly different geometrical conditions could explain the difference since it is well known that they might modify the features of the flow. Besides (PIV) visualizations (Goossens, 2005, p. 73, Fig. 3.24) at similar Reynolds number in a wind tunnel with a large blockage factor of $D/L_y = 10\%$ and a low aspect ratio of $L_z/D = 10$ of same order than the one used in SVV-LES also showed this secondary recirculation at the body upstream corners.

The spanwise velocity is found to be negligible outside the very near wall region and the agreement with experiments is as good as for the streamwise component, except for the first station at

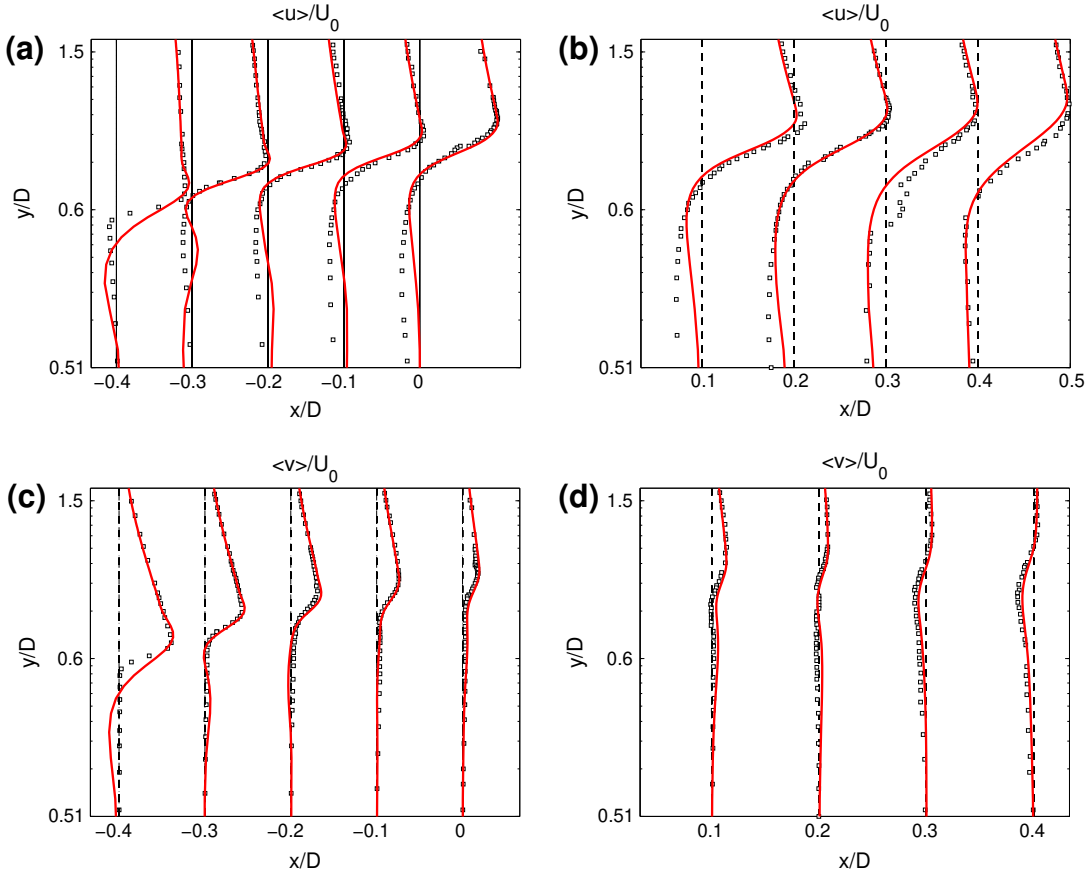

Fig. 6. Mean streamwise (a, b) and spanwise (c, d) velocity profiles from LDV measurements (squares) and SVV-LES (grid-1) (lines) at different locations in the streamwise direction for $Re = 21400$. (a and c) $x = -0.5$, $x = -0.4D$, $x = -0.3D$, $x = -0.2D$, $x = -0.1D$ and (b and d) $x = 0.1D$, $x = 0.3D$, $x = 0.4D$.

$x = -0.4D$ which is hard to precisely compute because of the corner. The maximum spanwise velocity is about $1.0U_\infty$ in upward region of the cylinder and it is about $-0.25U_\infty$ in the downward region.

Aerodynamics characteristics agree very well between experimental measurements and SVV-LES results. The lift and drag coefficients were determined by the wake survey method in the experiments and by integrating the pressure on the surface of the cylinder in the SVV-LES. The resulting drag coefficients and base pressure coefficients are equal to $Cd = 2.1$ and $Cp_b = -1.3$ for the measurements and $Cd = 2.2$ and $Cp_b = -1.3$ for the SVV-LES. This excellent agreement shows in particular that the SVV-LES well predicts the mean pressure distribution at the wall, which is one of the main ingredients in describing the cylinder wake (Williamson, 1996). Finally, SVV-LES estimates a Strouhal number equal to 0.141 that is 7% larger than the measured value, $St = 0.130$.

To examine turbulence distribution around the square cylinder, the two normal and the shear Reynolds stress tensor components are presented in Fig. 7 every 0.1D at several locations along the x the streamwise side face of the cylinder down to the first point at about $y = 0.51$D.

All the profiles show a satisfactory agreement between LDV and SVV-LES. The maximum of turbulence intensity is well located

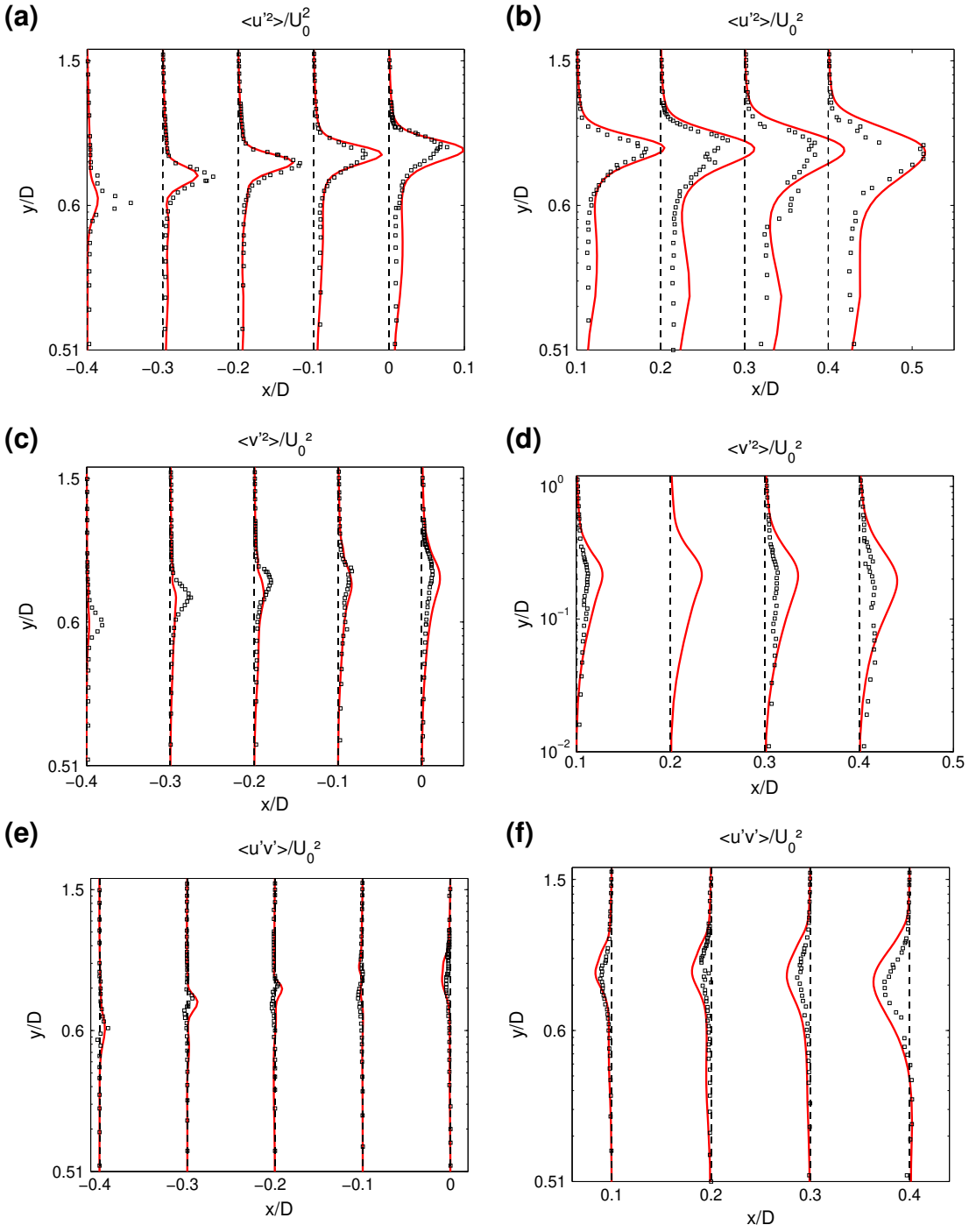

Fig. 7. Experimental LDV (squares) and SVV-LES (grid-1) (lines) normal and shear stress tensor components profiles at different locations in the streamwise direction for $Re = 21400$. (a, c, and e) $x = -0.5$, $x = -0.4D$, $x = -0.3D$, $x = -0.2D$, $x = -0.1D$ and (b, d, and f) $x = 0.1D$, $x = 0.3D$, $x = 0.4D$.

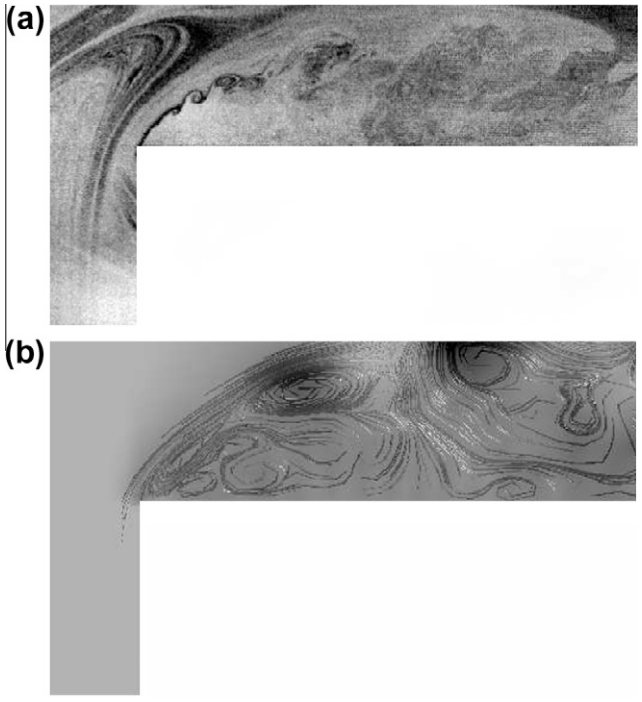

Fig. 8. Visualization of the KH structures in the flow. (a) By smoke, see Brun et al. (2008). (b) Instantaneous streamlines from SVV-LES (grid-2) in the *xy*-plane at $z = 2D$. Streamlines are calculated for seeds sowed in the near-wall region of the cylinder only. The white surface shows the whole top side of the cylinder of length D.

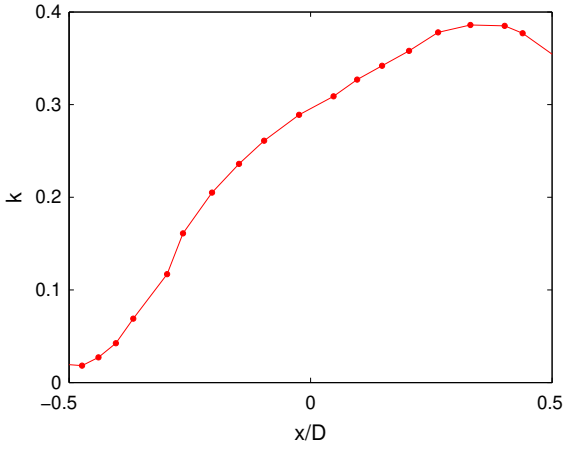

Fig. 9. Streamwise evolution of the maximum turbulent kinetic energy in the vertical direction showing the continuous increase of turbulence intensity along the shear layer, from SVV-LES (grid-1).

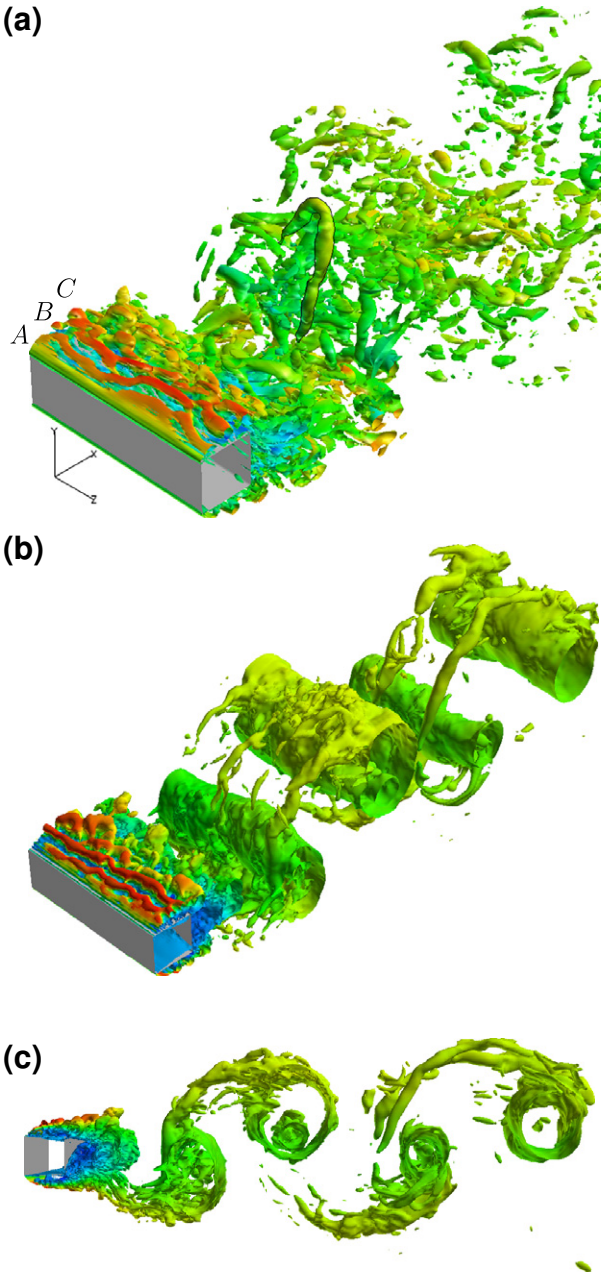

Fig. 10. Vortical KH and VK street structures for $Re = 21{,}400$, SVV-LES (grid-2). (a) Iso-surface of the Q-criterion colored by the streamwise velocity. (b and c) Iso-surface of low-pressure isovalue ($p/\rho U_\infty^2 = -0.9$) and pressure fluctuations ($p\prime/\rho U_\infty^2 = -0.15$) colored by streamwise velocity. A, B and C show the position where autocorrelations have been determined.

within the shear layer between the recirculation flow over the cylinder and the free stream. From $x/d = -01$ and along the downstream part of the cylinder surface, LES results fairly significantly overpredicts the turbulence intensity both in the very near-wall and in the shear layer as already observed in Fig. 4.

5. Transition to turbulence

Experimental flow visualizations and SVV-LES results agree to predict the development of three primary vortices related to the KH instability that are convected downstream as shown in Fig. 8 before pairing. SVV-LES solution and LDV measurements show that the shear layer gets unstable just above the upstream corner. The first KH structure developing in the shear layer is located experimentally at about $x = -0.45D$ and numerically at $x = -0.5D$ although this location is not accurately determined due to the high level of unsteadiness. Fig. 8 shows that SVV-LES predicts larger size vortices than visualizations that might indicate a locally excessive numerical dissipation induced by the discretization associated with the volume penalization of the cylinder in this very near-wall region.

To identify coherent three-dimensional vortices (Fig. 10), we use the pressure as well as the Q-criterion which defines a vortex as a spatial region where the Euclidean norm of the vorticity tensor $\Omega = \frac{1}{2}[\nabla V - (\nabla V)^t]$ dominates that of the rate strain $S = \frac{1}{2}[\nabla V + (\nabla V)^t] : Q = \frac{1}{2}[|\Omega|^2 - |S|^2] > 0$. The flow is characterized by large

scale vortices in the near wake due to the VK vortex street and by much smaller vortices developing in the shear layer above the cylinder triggering turbulence due to KH instability.

Flow structure shows that the KH instability produces very quickly slightly lifted spanwise vortices within the shear layer at the top of the cylinder. Indeed, only the first vortex is aligned on the cylinder upstream corner. The amplitude of the perturbation grows when the vortices are advected by the flow as shown by the profile of the RMS quantities calculated along the shear layer, Fig. 9.

Vortices eventually trigger turbulence before reaching the downstream corner of the cylinder. Vortices then break up into finer structures aligned with the spanwise direction before being stretched in the longitudinal direction and engulfed in the large scale VK vortex street in the rear of the cylinder as shown by the low-pressure isosurfaces (Fig. 10b and c). In the turbulent wake, Q-criterion surfaces (Fig. 10a) show fine disorganized structures superimposed around the VK vortex street with nevertheless at this instant a well-defined hairpin vortex.

Pressure isosurface shows that the primary VK vortex cores are wavy along the spanwise direction with a wavelength of about $2D$. Some much finer-scale streamwise vortices are pulled out from the primary vortices as observed at much lower Reynolds number during the transition by Williamson (1989). Although it is hard to determine the exact (spanwise) wavelength of the streamwise vortices, it should be around $0.3D$ slightly smaller than in the experiments of Williamson (1989) at much smaller Reynolds number.

Significant pressure fluctuations are located within the shear layer where the large VK spanwise vortices interact with the small streamwise ones (Fig. 10c). That indicates a significant level of turbulent kinetic energy in this region since the pressure fluctuations correlate excellently with the velocity fluctuations as shown experimentally by Tsai and Yang (1993) in a turbulent wake flow.

SVV-LES results show that the KH vortices combine with the recirculation bubble. The smallest vortices produce by the recirculation bubble along the upstream part of the cylinder surface move back to the upstream corner of the cylinder where they interact with the shear layer. These vortices are observed both in the mean (Fig. 5) and in the instantaneous streamlines (Fig. 8b). Such an observation, strongly unsteady, has already been observed for LES at lower Reynolds, $Re = 1500$, see works of Brun et al. (2008), but never at the present value of $Re = 21{,}400$. This process produces an energy feedback within the shear layer.

The temporal behavior of the flow is strongly unsteady particularly in the separated shear layer on the sides of the cylinder. Density energy spectra (Fig. 11) were computed on velocity samples and pressure at three stations extracted from the shear layer zone in the initial stage of the KH development close to the upper corner of the cylinder ($x = -0.45D$, $x = -0.40D$, and $x = -0.30D$, noticed A, B and C, respectively in Fig. 10a). Density energy spectra for the streamwise velocity and the pressure clearly show that KH instability and VK vortex act at different time scales.

The VK vortex frequency is the most energetic frequency observed at the three selected locations both in SVV-LES and in LDV. Second and third harmonics of this frequency are only observed in experiments at location B ($x = -0.4D$). At this station, a broad band frequency peak appears in the LDV measurements around $St = 6$ which represents the intermittent energy related to the KH vortical structures. In SVV-LES, this high frequency peak is less visible than in experiments probably due to a shorter integration time but a broad band frequency peak appears nevertheless around $St = 3.5$. On contrary to LDV, it seems present at all location confirming that the KH instability occurs earlier in the shear layer than in experiments whereas turbulence is triggered slightly later. These data provide a Strouhal ratio between the shear layer frequency and the fundamental VK frequency equal to 46 and 25 in LDV and SVV-LES, respectively. Further downstream in the flow at $x = 0.30D$ a first pairing has occured and leads to a broadening of the energy distribution in the low frequency direction. This is a typical backscattering effect observed in the initial transition phase of turbulent shear flows. The resulting energy spectra show a plateau in a large band from the VK frequency to the KH frequency. The computed frequency obtained in LES (about $St = 2$) is in the present experimental range. It might be possible that the shear layer frequency determined from the numerical results is affected by the near-wall numerical diffusion related to the SVV-LES method, resulting in a larger flow structure equivalent to what could be obtained at lower Reynolds number. With this respect, we consider the relation given in the literature for a round cylinder (Prasad and Williamson, 1997, 2005) between KH frequency and Kàrmàn frequency $f_{KH}/f_{VK} \propto Re^{0.67}$, and rebuild a lower effective Reynolds number for the simulation of the order of $Re = 9600$ instead of $Re = 21{,}400$ that may be considered in the very near-wall region.

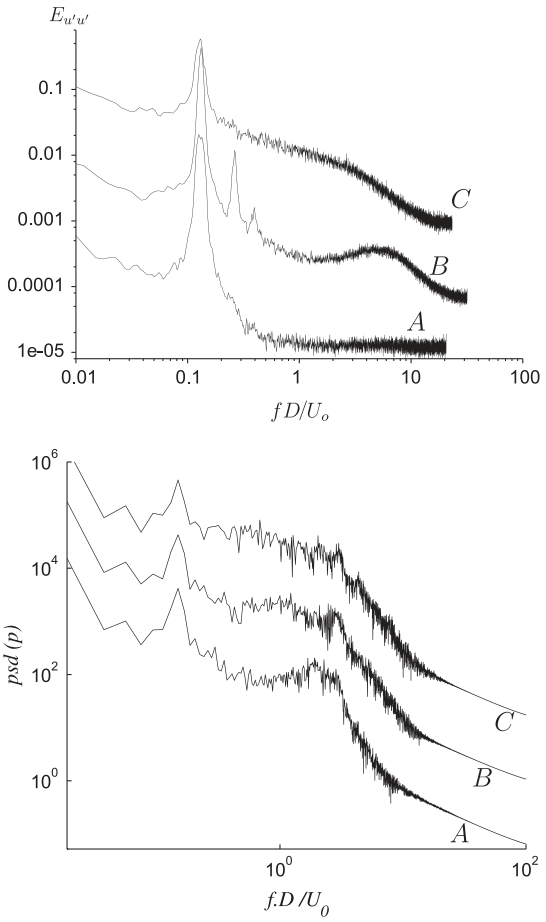

Fig. 11. Density energy spectra for the streamwise component (top) and the pressure (bottom) in the separated shear layer on the top of a square cylinder. LDV measurements (top) at $Re = 27{,}000$ from Brun et al., 2008 and SVV-LES (grid-1) results at $Re = 21{,}400$ at $[x = -0.45D; y = 0.63D]$, $[x = -0.40D; y = 0.63D]$, and $[x = -0.30D; y = 0.64D]$ from bottom to top and noticed A, B, C respectively. High frequency VK and low frequency KH peaks are clearly visible.

6. Concluding remarks

Instantaneous data and post-processed statistics were supplied from experimental LDV measurements and SVV-LES results of the turbulent flow around a square cylinder for th ERCOFTAC Reynolds

number $Re = 21{,}400$. High spatial resolution close to the cylinder wall has been provided down to $y/D = 0.01$ and $z/D = 0.125$ to specially focus on the transition that takes place in the separated shear layers developing over the upper surface of the body. This was necessary to provide an overall agreement on the turbulent statistics and on the flow topology in the separated shear layers. SVV-LES well predicts the maximum of turbulence intensity within the shear layer but globally overpredicts the turbulence intensity. A sufficient time resolution allowed to tackle unsteadiness from quasi periodic large VK vortex street to small inhomogeneous scales and intermittent turbulence related to KH instability in the separated shear layer. SVV-LES results capture for the first time numerically in turbulent regime the high frequency range related to the KH instability, even if a local extra diffusion provided by the discretization and the penalization technique in this very near-wall region leads probably to an excessive local dissipation that might explain the underestimation of the KH frequency. The global low numerical dissipation of the spectral approximation associated to the proper resolution of all these ingredients give the opportunity to provide the correct large scale behavior of the flow in the whole wake behind the cylinder. Mainly, drag coefficient, Strouhal number, base pressure coefficients were correct thanks to a correct description of the shear layer around the cylinder, which had never been numerically modeled for such case before.

In conclusion, the present work extends former studies of the literature with resolving the very near-wall surface of the cylinder. The observed differences between SVV-LES and LDV measurements show however that development work is still needed to improve numerical predictions.

Acknowledgments

SVV-LES was granted access to the HPC resources of IDRIS under the allocation 2010-0242 made by GENCI (Grand Equipement National de-Calcul Intensif). The work was supported by CNRS in the frame of the DFG-CNRS program "LES of complex flows". ES acknowledges support from Spanish Government through research projet FIS2008-01126.

References

Bloor, M.S., 1964. The transition to turbulence in the wake of a circular cylinder. J. Fluid Mech. 19, 290.

Bosch, G., Rodi, W., 1996. Simulation of vortex shedding past a square cylinder near a wall. Int. J. Heat Fluid Flow 17, 267–275.

Bosch, G., Rodi, W., 1998. Simulation of vortex shedding past a square cylinder with different turbulence models. Int. J. Numer. Meth. Fluids 28, 601–616.

Brun, C., Goossens, T., 2008. Coherent vortices in the turbulent near wake of a square cylinder. C.R. Mécanique 336, 363–369.

Brun, C., Aubrun, S., Goossens, T., Ravier, Ph., 2008. Coherent structures and their frequency signature in the separated shear layer on the top of a square cylinder. J. Flow Turb. Comb. 81, 97–114.

Dong, S., Karniadakis, G.E., Ekmecki, A., Rockwell, D., 2006. A combined direct numerical simulation-particle image velocimetry study of the turbulent near wake. J. Fluid Mech. 569, 185–207.

Durao, D.F.G., Heitor, M.V., Pereira, J.C.F., 1988. Measurements of turbulent and periodic flows around a square cross-section cylinder. Exp. Fluids 6 (5), 298304.

Franke, R., Rodi, W., 1991. Calculation of vortex-shedding past a square cylinder with various turbulence models. In: Proceedings 8th Symposium on Turbulent Shear Flows, Munich, paper 20-1.

Gerrard, J.H., 1966. The mechanics of the formation region of vortices behind bluff bodies. J. Fluid Mech. 25, 401–413.

Goossens, T., 2005. Etude expérimentale et numérique du sillage turbulent et des forces instationnaires sur un obstacle bi-dimensionnel non profilé. PhD thesis. Orléans university.

Iaccarino, G., Ooi, A., Durbin, P.A., Behnia, M., 2003. Reynolds averaged simulations of unsteady separated flow. Int. J. Heat Fluid Flow 24 (2), 147–156.

Lübcke, H., Schmidt, St., Rung, T., Thiele, F., 2001. Comparison of LES and RANS in bluff-body flows. J. Wind Eng. Ind. Aero. 89, 1471–1485.

Lyn, D.A., Rodi, W., 1994. The flapping shear layer formed by the flow separation from the forward of a square cylinder. J. Fluid Mech. 267, 353:376.

Lyn, D.A., Einav, S., Rodi, W., Park, J.H., 1995. A laser doppler velocimetry study of ensemble averaged characteristics of the turbulent near wake of a square cylinder. J. Fluid Mech. 304, 285–319.

Minguez, M., Pasquetti, R., Serre, E., 2008. High-order large-eddy simulation of flow over the Ahmed body car model. Phys. Fluids 20 (9), 095101–095101-17.

Okajima, A., 1982. Strouhal numbers of rectangular cylinders. J. Fluid Mech. 123, 379–398.

Pasquetti, R., Severac, E., Serre, E., Bontoux, P., Schaefer, M., 2008. From stratified wake to rotor–stator flows by a SVV-LES method. Int. J. Theor. Comput. Fluid Dyn. 22 (3-4), 261–273.

Patankar, S.V., Kelkar, K.M., 1992. Numerical prediction of vortex shedding behind a square cylinder. Int. J. Numer. Meth. Fluids 14, 327–341.

Prasad, A., Williamson, C.H.K., 1997. The instability of the shear layer separating from a bluff body. J. Fluid Mech., 333–375.

Rajagopalan, S., Antonia, R.A., 2005. Flow around a circular cylinder-structure of the near wake shear layer. Exp. Fluids 38, 393–402.

Rodi, W., 1993. Comparison of LES and RANS calculations of the flow around bluff bodies. J. Wind Eng. Ind. Aerodyn., 3–19.

Sohankar, A., Davidson, L., Norberg, C., 2000. Large Eddy Simulation of the flow past a square cylinder : comparison of different subgrid scale models. J. Fluid Eng. 122, 39–47.

Tsai, G.-L., Yang, J.-T., 1993. Pressure fluctuation in correlation with velocity fluctuations in turbulent wake flow. Exp. Fluids, 462–463.

Voke, P., 1996. In: 2nd ERCOFTAC Workshop on Direct and Large-Eddy Simulation. Grenoble.

Wei, T., Smith, C.R., 1986. Secondary vortices in the wake of circular cylinders. J. Fluid Mech. 169, 513.

Williamson, C.H.K., 1989. Oblique and parallel modes of vortex shedding in the wake of a cylinder. J. Fluid Mech. 206, 579–628.

Williamson, C.H.K., 1996. Vortex dynamics in the cylinder wake. Ann. Rev. Fluid Mech. 28, 447–539.